Bands, bonds, and charge-density waves in the $NbSe_3$ family of compounds

J. A. Wilson
Bell Laboratories, Murray Hill, New Jersey 07974
(Received 30 October 1978)

Through detailed examination of the crystal structure and bonding conditions in the trichalcogenides, it has been possible to gain a deeper understanding of the band structure of these complex materials, and with this of their unusual electronic behavior. The character of the observed semimetallicity in $TaSe_3$ and $NbSe_3$ is much clarified. Each material in the group-V family is seen to achieve a very individually tailored band structure, enfolding the various structural and energy-level adjustments. The nonuniformity and the molecularization of these structures contrasts strongly with the dichalcogenide behavior. The structural, if not the electronic, dimensionality of the group-V trichalcogenides remains closer to two than to one. It is found that the periodic structural distortions developed by $NbSe_3$ are probably more suited to a metal-metal bonding description than to the traditional Fermi surface determined instability of a charge-density wave. The field-induced sliding of these distortions can then be described in terms of cooperative bond flipping through a discommensurate superlattice. We examine in crystal chemical terms why this motion is so unusually weakly pinned to defects and impurities in $NbSe_3$. In fact, the investigation shows that it will be very hard to find a material better suited to the realization of this phenomenon.

I. INTRODUCTION

Many papers[1-30] have appeared recently in connection with the physical properties of the transition-metal trichalcogenides, in particular those of $NbSe_3$. The special interest lies in the fact that the two "charge-density waves" (CDW) forming in $NbSe_3$ (onset temperatures $T_{d1} = 144$ K, $T_{d2} = 59$ K) can, it seems, be induced to slide through the material under the application of a very modest electric field gradient ($\gtrsim 0.1$ V cm^{-1}).[8,10] We are given to understand that the incommensurate CDW's in $NbSe_3$ are unusually weakly pinned to the lattice.[31-34] Indeed already by microwave excitation frequencies of 10 GHz (0.05 meV) they have become free to carry current.[10] This restores the level of conductivity in the material to a value close to what would have obtained had the Fermi surface never been partially gapped under the action of these CDW's. Relatively little attention has been given as to why, out of all the various CDW-bearing materials, this phenomenon should show up only in $NbSe_3$. Indeed little crystal chemical discussion has been given concerning why the four materials NbS_3, $NbSe_3$, TaS_3, and $TaSe_3$ present very individualistic behaviors, while the corresponding dichalcogenides[35] behave as a unit. This we try to remedy.

The crystal structures of the group-V trichalcogenides are more complicated than those of the layer-structured dichalcogenides. In the latter there is only one type of metal atom per cell (normally), whereas in $NbSe_3$ there are three. Moreover, despite all four materials holding to a common structural element (the trigonal prismatic column), the structure of each material differs significantly in detail. The related d^0 group-IV trichalcogenides by contrast are isostructural from TiS_3 (Ref. 1) to $ThTe_3$ (Ref. 36). The structural differences in group V involve the accompaniment of major qualitative changes in electronic band structure, and indeed even the electronic configuration of the cations. Thus, using the customary loose designations, NbS_3 is a 4+ d^1 compound, with properties and form[20] much as expected given those of d^0 ZrS_3,[1-3] while $TaSe_3$ is in essence an empty d-band compound (though displaying a slight semimetallic p-d overlap).[12,36,37] The lack of full structural continuity for group-V trichalcogenides one to the next, and furthermore to the group-IV family, has restricted attempts to grow mixed crystals; a procedure that in the dichalcogenides helped greatly to resolve the nature of the observed lattice instabilities.[35]

Before looking at the various crystal structures and electronic states in detail, two points should be emphasized here. First, the group-V trichalcogenides are not half-filled band metals. In this they are not like the dichalcogenides. Indeed the latter are always paramagnetic above T_d, and even below T_d in the $2H$ case, while the trichalcogenides are each diamagnetic at all temperatures.[4,27,37(a),38] For the latter the Hall constants are appropriately several orders of magnitude the larger.[28] The second point is that the trichalcogenides are not one-dimensional compounds in the sense that $K_2Pt(CN)_4Br_{0.3}nH_2O$ (Ref. 39) is, or NbI_4,[40] or $V(S_2)_2$.[41] Very substantial structural cross-linking occurs between the chains, the M-X coordination in the trichalcogenides moving towards 8 [as for $PuBr_3$ or ThI_4 (Ref. 36)] rather than 6 (as in the dichalcogenides, or NbI_4). For example, in $ZrSe_3$,

besides the six "intrachain" bonds ~2.73 Å, there are two interchain bonds ~2.87 Å.[1] As a result, the materials are as close to being layer structures as to chain structures in the true sense [distinct from what has passed for chains in, say, NbO_2 (Ref. 42) or Nb_3Sn (Ref. 43)]. Even the recently measured anisotropy ~20 *within* the slabs for $NbSe_3$ (Ref. 29) (i.e., containing axes b and c) is, we shall see later, likely still to suggest a greater degree of one dimensionality for the material than really exists. It would be interesting to have this anisotropy measured again in the simpler structural and electronic condition supplied by $ZrSe_3$.

II. COMPARATIVE DESCRIPTION OF THE CRYSTAL STRUCTURES

Two factors affect the evolution of the structures of the group-V trichalcogenides from that of the group-IV prototype $ZrSe_3$.[1] First, there is metal-metal bonding, which can lead to uniaxial cation-cation pairing along the chain direction. This occurs with NbS_3,[20] and puts the material in line with many other d^1 compounds like α-NbI_4 (Ref. 40) and $Nb(S_2)Cl_2$ (Ref. 44) or $V(S_2)_2$ (Ref. 41) and VO_2.[45] The Nb-Nb distance within the b-axis pair in NbS_3 is 3.04 Å compared with 3.36 Å if there were no pairing. Such pairing succeeds in many cases in dropping a filled subband off from the bottom of the d-band manifold to leave a small gap (~1 eV) semiconductor. The Seebeck coefficient for NbS_3 is ~500 μV/°C.[38] The second factor, actually more prevalent in the present materials, is to adjust the structure so that some (in $NbSe_3$) or all (in $TaSe_3$) of the cations become pentavalent.[36] It is quite easy for the present form of structure to accomodate the necessary augmentation to the electron content of the chalcogen-based valence band, as we will see. It is well known, as can be appreciated from Fig. 1, that $ZrSe_3$ is effectively $Zr^{4+}(Se_2)^{2-}Se^{2-}$. The $(Se_2)^{2-}$ pairing leads to a tightly bound valence subband, very evident in the x-ray photoemission (XPS) results,[3] and there is correspondingly the ejection of an antibonding state up out of the p band. This leaves a 16- rather than an 18-electron p valence band. The Se-Se_2 pair in $ZrSe_3$ is as strong (2.35 Å) as in pyrite-structured $MnSe_2$, where it was evident that the antibonding p state is ejected as much as 5 eV above the top of the occupied p band.[46]

In the case of group-V triselenides some of the -Se_2 become to varying degree unpaired, and certain of the antibonding p states fall back below the Fermi level in the bottom of the d band. Further electrons pass over then from one or more of the cation sublattices to the anion sublattice. Because

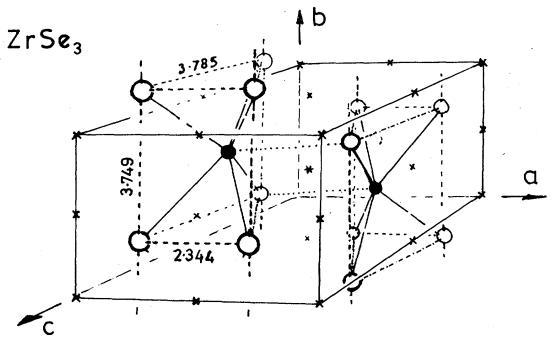

FIG. 1. Monoclinic cell of $ZrSe_3$ showing staggered prismatic columns and their crosslinking. Lengths in angstroms. Note how tightly back wall of prism is drawn in by Se_2 pairings. Prisms should be slightly taller than drawn. All atoms at $y = \pm\frac{1}{4}$. Centers of inversion here and in remaining figures marked by cross.

of the interchain cross-linking shown by the structures, the various cation sublattices (chain types) are not independent, and partial valencies (between 4 and 5) may develop for the cations on all sublattices. However, before one can properly appreciate the electronic structures, it first is necessary to study in greater detail the specific structures actually acquired.

(i) $ZrSe_3$. Figures 1 and 2 show how the formulation $Zr(Se_2)Se$ and an empty d band arises. The p- to d-band gaps in the *tri*chalcogenides[1(b),2] are almost identical with those in the corresponding dichalcogenides.[47] In $ZrSe_3$ the gap is 1.1 eV, in ZrS_3 it is 1.9 eV. Typically, in the *di*chalcogenides

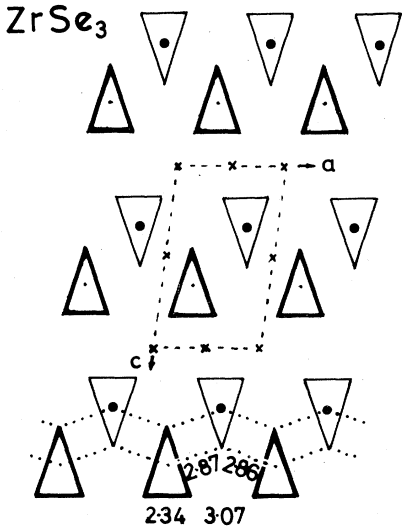

FIG. 2. Plan of Fig. 1. Each unit cell forms part of slab in a-b plane two columns thick. Zr-Se range in prisms from 2.72–2.74 Å. Heavy atoms at $\frac{1}{4}b_0$; light at $\frac{3}{4}b_0$.

between groups IV and V, the d band is lowered by 1 to $1\frac{1}{2}$ eV so that slight p-d overlap is present in $1T(2H)$-$TaSe_2$, etc., but the degree of d-band filling is great enough there for the Fermi level to lie only in the d band. Such a situation is not likely to persist in the group-V *tri*chalcogenides due to modification from M-M and X-X pairings, as we shall see.

In Fig. 2 the interchain couplings are dotted in. These form a continuous M-X-M-X pathway perpendicular to the columns, and must be taken into account when the band structure comes to be calculated. In the closely related $PuBr_3$ structure,[36] where no anion-anion pairing occurs and the cation is trivalent, the trigonal prismatic columns pack into narrower slabs, with the interchain linkages now immediately terminating on the "back" edge of the prisms [see Fig. 3(a)]. Similar packing to this recurs, as we shall see, in the structures of $NbSe_3$ and $TaSe_3$ at those columns which show no anion-anion pairing.

Further drawing attention to the cross linkages is the existence of a second variant B of the $ZrSe_3$-

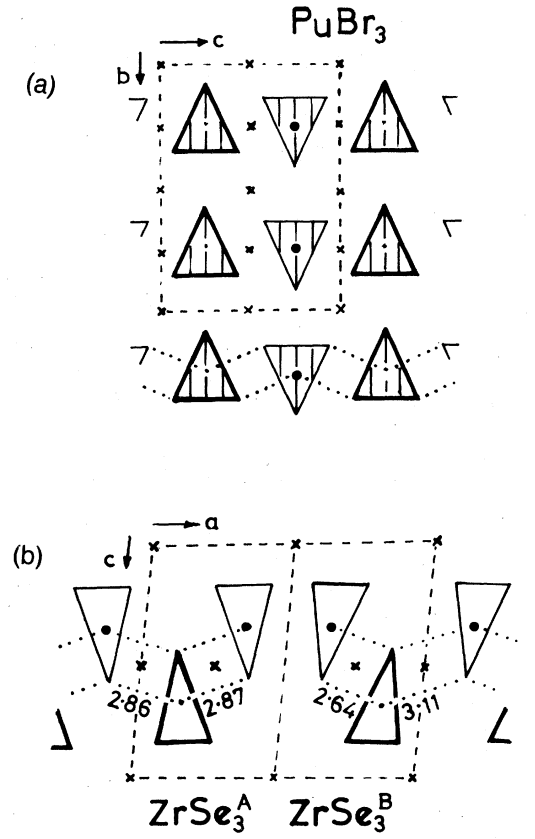

FIG. 3. (a) Orthorhombic $PuBr_3$ structure. Prismatic columns now fully interpenetrate slabs. Space group D_{2h}^{17}, with origin at $2/m$. Heavy atoms at $x=0$; light atoms at $x=\frac{1}{2}$; (b) two variants of $ZrSe_3$ structure, emphasizing change in intercolumn pathways.

type structure,[1(a)] measured for TiS_3, $HfSe_3$, and $ZrTe_3$ [Fig. 3(b)]. Here the two interchain M-X distances, which are almost identical in $ZrSe_3^A$ at at 2.870 and 2.868 Å, become highly differentiated, being in $HfSe_3^B$ for example 3.100 and 2.624 Å. The shorter distance is now indeed less than the average M-X bond length *within* the prism.

(ii) NbS_3. The distortion of the $ZrSe_3$ structure developed by NbS_3,[20] being in the form of intrachain cation pairing, becomes of prime interest to the present work. Such pairing is endemic to t_{2g}^1 (or t_{2g}^5) chains, whether metallic initially as in VO_2,[45] or insulating[46] as in low-spin d^5 $RuBr_3$. (A satisfactory structural analysis has not yet been made for $d^1\beta$-$TiCl_3$, etc.) Accordingly, the form of the distortion is not governed by the Fermi-surface geometry, but by optimization of intercellular matrix elements. In NbS_3 the pairing represents a 10% reduction in cation spacing under b-axis shifts of 0.16 Å. The bridging triangle of sulphur atoms is pushed outwards in an attempt to conserve M-X bond lengths, the principal factor determining the energetics of the main p-valence band. (See Ref. 48 for case of dichalcogenide periodic structural distortions.) The triangle at the other end of the prism is correspondingly drawn in. In neither triangle, however, does the dimension of the S_2^{2-} pairing deviate from what is to be expected, given that in ZrS_3 (see Table I).

The band gap generated with the cation pairing in NbS_3 has not been ascertained yet, but is likely to be no more than $\frac{3}{4}$ eV, and so is $d \rightarrow d$ (as in VO_2) rather than $p \rightarrow d$. If the triselenide had adopted this structure such would probably no longer be the case.

(iii) $TaSe_3$. This material shows a very different evolution of the $ZrSe_3$ structure, as is to be seen from Fig. 4 and Table I. The slabs break up into canted blocks of four columns each.[37(b)] These blocks are composed of an inner duo of columns that are still in the $ZrSe_3$ setting, and display fairly substantial X-X pairing (2.58 Å). The flanking duo, however, have almost completely relaxed their X-X pairing (2.90 Å to be compared with 3.43 Å in $TaSe_2$). Moreover, the intercolumn linkages now terminate on these expanded columns instead of forming extended pathways. These terminations here occur at both the back edge and front corner of the prism, unlike the situation in $PuBr_3$ (back edge only).

For convenience of reference here and later, we shall designate the columns with little or no X-X pairing "red," columns with intermediate X-X pairing "orange," and the columns with tight X-X pairing (as in $ZrSe_3$) "yellow." In $NbSe_3$ we shall find all three types.

The first set of columns in $TaSe_3$ is "orange,"

TABLE I. Crystallographic data for trichaleogenides.

	a_0 (Å)	b_0 (Å)	c_0 (Å)	β	Z	Space group	Molecular volume (Å^3)	Anion pair lengths (Å) Intrachain	Shorter interchain	Reference
$ZrSe_3$	5.411	3.749	9.444	97.48°	2	$P2_1/m$ (C_{2h}^2)	94.97	2.344	3.067	1(b)
$NbSe_3$	10.009	3.480	15.629	109.47°	6	$P2_1/m$ (C_{2h}^2)	85.55	2.374 2.485 2.909	2.73 2.93	21
$TaSe_3$	10.402	3.495	9.829	106.26°	4	$P2_1/m$ (C_{2h}^2)	85.76	2.58 2.90	2.65	37(b)
ZrS_3	5.124	3.624	8.980	97.28°	2	$P2_1/m$ (C_{2h}^2)	82.84	2.090	3.035	3(a)
NbS_3	4.963	6.730	9.144	97.17°	4	$P\bar{1}$ (C_i^1)	75.75	2.05	2.91	20
TaS_3	36.804	15.173	3.340	90°	24	Not known	77.71	Not known		13

[a]Note prismatic chains are parallel to b axes in each case except TaS_3 where parallel c.

[b]In the refinement of the structure of NbS_3 (Ref. 20) the centers of inversion have not been chosen as origin, but a point halfway between these.

[c]In $NbSe_2$ 1.948×10^{21} cells/cm^3; in $TaSe_3$ 2.915×10^{21}. Multiply these by 2 for density of electrons needed to fill a particular band.

its X-X pairing at 2.58 Å being considerably weaker than in $ZrSe_3$ (2.34 Å) or in the pyrites $MnSe_2$ (2.38 Å), and $OsSe_2$ (2.44 Å) or the marcasite $FeSe_2$ (2.53 Å).[49] (N.B., the latter two compounds are t_{2g}^6 semiconductors.) The pairing in $TaSe_3$, however, is, as strong as that in $IrSe_2$, for which a constitution $Ir_8^{3+}(Se^{2-})_8(Se_2)_4^{2-}$ with t_{2g}^6-e_g^0 semiconductivity is still secured (see Ref. 47, Fig. 10). The pairing evidently remains sufficiently strong to cast the antibonding p state the 1 or 2 eV above the top of the occupied p band that is needed.

Because of the above rather weak Se-Se bonding in the columns of $TaSe_3$, an *inter*column Se-Se separation of only 2.65 Å is incurred, as compared with 3.07 Å in $ZrSe_3$. This may well be short enough significantly to perturb the top of the p-band structure, as will be seen presently.

(iv) $NbSe_3$. The structure of $NbSe_3$ (Ref. 21) includes similar blocks of four columns to those in $TaSe_3$ (though with the inner "orange" columns showing somewhat stronger Se-Se pairing), but these blocks are now interconnected through an additional duo of strongly canted $ZrSe_3$-like "yellow" columns instead of being directly linked (Fig. 5). The interchain M-X pathways once again terminate at the red columns. The slab cleavage plane, though not kinked as in $TaSe_3$, cuts through some rather short red-to-yellow spacings of 3.30 Å. The yellow columns define interslab slices in the a-b plane, and inclined yellow-orange sheets may also be traced. Within the true slab planes (b-c) the path between the yellow and orange columns is of course interrupted by the red columns.

(v) TaS_3. The crystal structure for the last member of the family (no group-V tritellurides are known) is not yet fully determined. It has been reported that the cell contains 24 molecular units and is face-centered orthorhombic.[13,37(b)] The originally ascribed space group D_2^5 had no centers of inversion, and this was difficult to reconcile with the present class of structures. The very recent work of Tsutsumi[50] suggests D_{2h}^{17}. This is actually the space group for $PuBr_3$,[36] but it still seems to offer difficulties for TaS_3 with $Z=24$. $TaSe_3$, as a glance at Fig. 4 will show, almost presents a face-centered-orthorhombic cell of eight-molecule content, spanning two slabs. The actual angle there to the four-column-broad unit was 93.38°. Cell dimensions quoted for TaS_3,

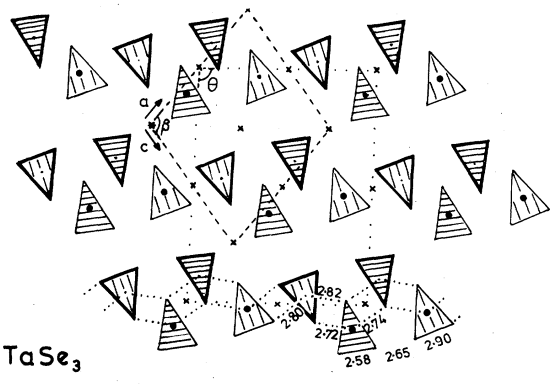

FIG. 4. Plan of $TaSe_3$ structure. Heavy features at $y=\frac{1}{4}$, light at $y=\frac{3}{4}$; orange column, ▽; red column, ▲; $\theta=93.38°$. Ta-Se range in prisms 2.60–2.65 Å [Ref. 1(a)].

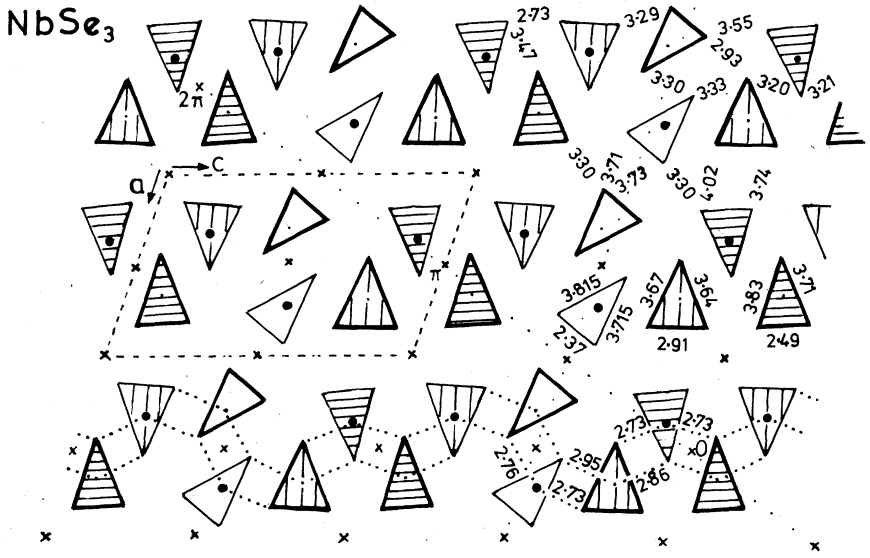

FIG. 5. Plan of $NbSe_3$ with details as determined in Ref. 21. *b* axis *into* paper. Heavier features at $y=\frac{3}{4}$; light at $y=\frac{1}{4}$. Nb-Se range in prisms 2.63–2.67 Å. △ yellow (fully paired), ▲ orange, ⚠ red (depaired). Yellow columns in rows parallel to a_0; orange in rows parallel to ⟨101⟩.

seem to be for a 2 slab × 12 column unit.

The material clearly does not show *M*-*M* pairing in the columns (unlike NbS_3) since its *c*-axis parameter corresponds to the height of one prism only (at 300 K). TaS_3 should, however, show a stronger adherence to *X*-*X* pairing than $TaSe_3$ and therefore be more 4+ like. Nonetheless it is quite strongly diamagnetic, even at room temperature,[37(a)] so that, as with all these materials, the number of free carriers that is finally presented is rather small.

We now turn to look in more detail at the electronic properties, their form, and their origin.

III. GENERAL FORM TO THE BAND STRUCTURES AND THE RESULTING ELECTRONIC CONDITIONS

When the number of molecules per unit cell becomes large and of "differentiated disposition," and particularly as the space-group symmetry becomes rather limited, the band structure is rapidly brought to a state of horizontal stratification. The many bands, often not degenerate even at the special points in the zone, are held from crossing each other under the very restricted set of symmetry representations prevailing. This is particularly so once the double-group representations are considered.

A feeling for the type of situation to be expected in $ZrSe_3$ or $TaSe_3$ can be gained from the calculated band structure for VO_2 in its room-temperature monoclinic state (Ref. 45, Fig. 2). Only the rather isolated *M*-*M* bonding *d* band reaches 1 eV in width. The space group for monoclinic VO_2 ($Z=4$) is C_{2h}^5. As in the present case with C_{2h}^2, very few degenerate representations arise, though there is

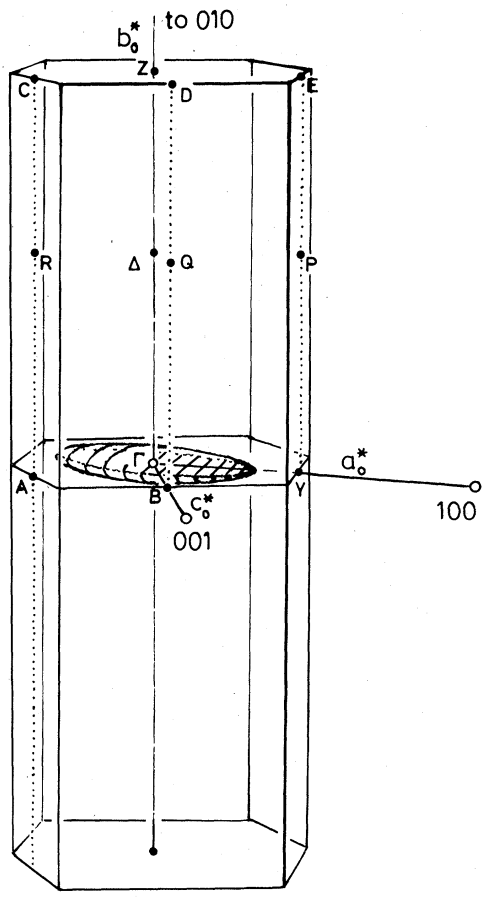

FIG. 6. Brillouin zone for $NbSe_3$ to scale. Plan in Fig. 7(b). Fermi surface shown produces a 1% zone filling—see text.

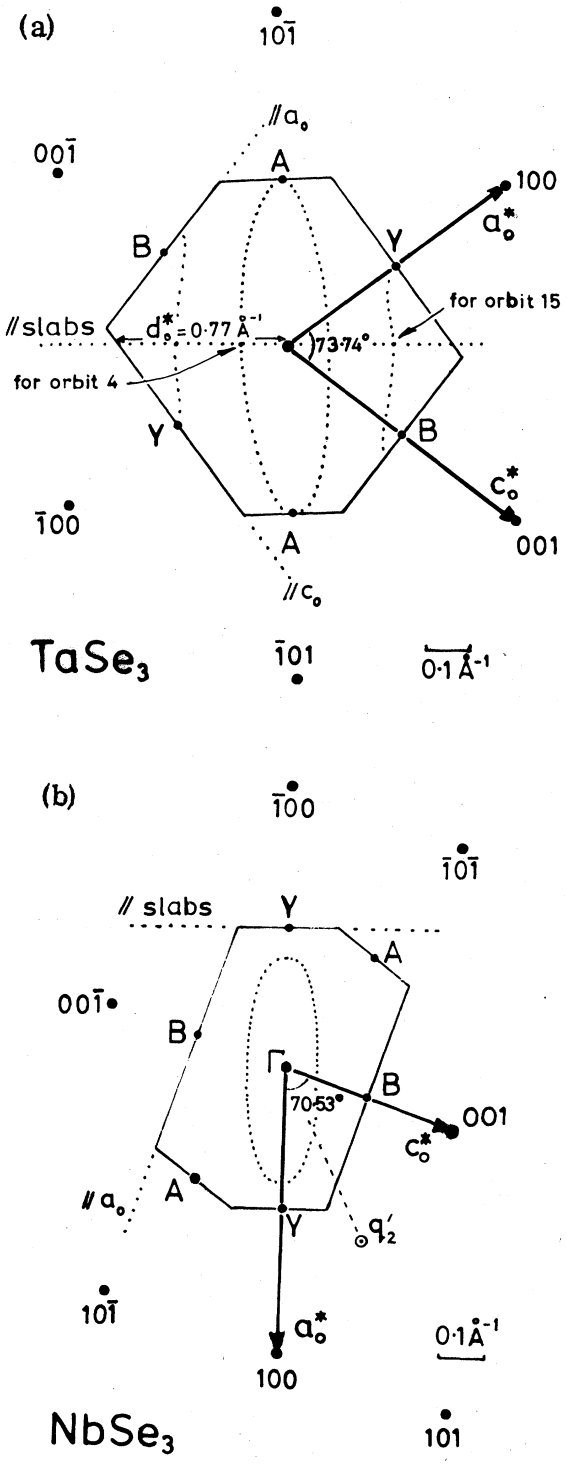

FIG. 7. (a) Brillouin zone for $TaSe_3$ in plan, in orientation corresponding to Fig. 4. The orbits indicated are *in* the plane of the slabs (i.e., containing b^*); (b) Brillouin zone for $NbSe_3$ in plan, in orientation corresponding to Fig. 5 (i.e., b^* axis into paper). Fermi surface shown is that which appears in Fig. 6 for 1% zone filling.

some degeneracy associated with time reversal symmetry. Away from the points of special symmetry there are never more than two representations. The Γ point with little group $P2/m$ and elements E, I, $C_2^{(y)}$, and $\sigma^{(xz)}$ has four singly degenerate representations. Some points like Z have just a lone doubly degenerate representation.

The monoclinic zone, given proportions appropriate to $NbSe_3$ (and Zak's labeling of the symmetry points) is shown in Fig. 6. The cross sections of the zone perpendicular to b^* (i.e., to b_0 the chain direction) are shown for $TaSe_3$ and $NbSe_3$ in Fig. 7. These cross sections have been shown in the orientation appropriate to Figs. 4 and 5 for the crystal structures, meaning the direction corresponding to the slab-plane runs "east-west." [Note for $NbSe_3$, in order to obtain a right-hand set of axes, b_0 and b^* are directed *into* the paper in Figs. 5 and 7(b).]

The seemingly higher symmetry to the $NbSe_3$ zone is coincidential and is due to the approximately equal disposition of [100] and [101] about [201] (the origin of which is illustrated in Ref. 21). Even with $TaSe_3$, points Y, B, and A appear midleadingly close to the midpoints of the zone faces. There is, of course, no mirror plane *parallel to* b^*. The dimensions of the zones are given in Table II.

The *general* sort of shape to be anticipated for a small piece of Fermi surface in these materials is portrayed in Fig. 6. There is strong elongation perpendicular to the slab direction because of low band dispersion in this direction across the Van der Waals gaps. Within the plane of the slabs, particularly for a p-band surface, we expect ellipsoidal sections of relatively small eccentricity. It should be noted from Fig. 5 that the typical Se-Se distance in the slabs $\perp b_0$ (~3.30 Å) is actually less than the Se-Se distance along the columns (3.48 Å). Since much of the width of a d band in materials like the present comes from p-d mixing,[51] initial "d-band" curvatures in the slab are likely to be comparable, despite metal-metal spacings between columns being at ~4.3 Å considerably greater than those in the columns (3.49 Å). It should be noted that in the very good pyrite metal β-$RhSe_2$ (e_g^1) the shortest metal-metal distance also is 4.3 Å.[47] The "d-band" width does not depend primarily on this direct M-M overlap.

In accord with the above, a tentative measure of the effective masses indicates there to be little anisotropy in the slabs for the very small number of carriers present in $NbSe_3$ at helium temperatures, while perpendicular to the slabs an anisotropy of 3 in mass is reported.[11] The room-temperature conductivity anisotropy σ_b/σ_a in $NbSe_3$ is ~500,[9] whereas the "in slab" σ_b/σ_c is only ~15.[29] These values probably are somewhat overstated because of the very easy crystal fracture parallel

TABLE II. Reciprocal-space details for $TaSe_3$ and $NbSe_3$.

	a^* (Å^{-1})	c^* (Å^{-1})	b^* (Å^{-1})	β'(deg)	Volume of zone (Å^{-3})	Area of zone basal plane (Å^{-2})	Megagauss equivalence (MG)	Area of b^* containing section parallel to slabs (Å^{-2})	Megagauss equivalence (MG)
$TaSe_3$	0.6292	0.6659	1.7978	73.74	0.7231	0.4022	42	1.38	145
$NbSe_3$	0.6658	0.4264	1.8055	70.53	0.4832	0.2676	28	0.77	80

to b.

As evaluated in Table I, a 1% filled band or zone in $NbSe_3$ would amount to 3.9×10^{19} e/cm^3. The ellipsoid drawn in Fig. 6 is of approximately this filling, met by semiaxes $\frac{2}{5}a_0^*$, $\frac{1}{5}c_0^*$, $\frac{1}{35}b_0^*$ (i.e., 0.266, 0.085, 0.051 Å^{-1}). The experimental room-temperature Hall coefficient[19] of -1×10^{-2} cm^3/cb, were it attributable simply to n-type carriers, is equivalent to only 1.5×10^{19} e/cm^3, so that even prior to the CDW transitions the material is very much the semimetal with $\sim\frac{1}{2}$% band filling. [The susceptibility, while quite strongly negative (-0.21×10^{-6} emu/g),[27] is appreciably larger than in $ZrSe_3$ (-0.33×10^{-6}),[1(b)] but there are going to be several additional paramagnetic terms besides the Pauli term, itself enhanced in $NbSe_2$.] The CDW transitions in $NbSe_3$ seem to remove about 75% of the Fermi surface,[10] taking the carrier count down to only $\lesssim4\times10^{18}$/cm^3, or 0.10% zone filling. The above concentrations are even less than in $TiSe_2$ (Ref. 52) above and below its electron-hole driven condensation, and the details are intrinsically even more difficult to analyze fully, as we shall see.

We turn now to consider in some detail the electronic conditions established in the three materials $TaSe_3$, $NbSe_3$, and TaS_3.

(i) $TaSe_3$. $TaSe_3$ shows no low-temperature distortions and loss of free carrier content. From its somewhat lower diamagnetism and higher conductivity at 300 °K the carrier content would appear a little greater than in $NbSe_3$. Some Shubnikov–de Haas data has been collected for $TaSe_3$ for orbits in the plane of the slabs, and also for their variation in "area" upon inclining the field to produce tilted *inter*slab orbits. As might have been expected, the observed angular response function is of the form to characterize the Fermi-surface cross sections sampled as coming from effectively cylindrical elements, the situation in a layer compound (see Ref. 16, Fig. 12, where the common cylindrical axis falls closely perpendicular to the slabs; compare Fig. 7 in Ref. 56 dealing with the Fermi surface of 2H-$TaSe_2$). Most of the orbits are quite small, even orbit 15 amounting to only about $\frac{1}{10}$ the area of the relevant b_0^*-containing section of the zone [closely parallel to the slabs; see Fig. 7(a)].

In the SdH data the area of orbit 15 would be satisfied by an ellipse with semiaxes $0.20\times(\frac{1}{2}b_0^*)$ by $0.66\times(\frac{1}{2}d_0^*)$, (i.e., 0.18×0.24 Å^{-1}). Such a cylinder is included in Fig. 7(a), and amounts to a zone filling of approximately 10%. From Table I, we see this takes an electron density of about 5 or 6×10^{20}/cm^3, which is very comparable to that in $TiSe_2$ at room temperature.[52] Orbit 4, which is $\frac{1}{5}$ the size of orbit 15, would be satisfied by an elongated ellipsoid that just reaches point A [see Fig. 7(a)], the cross sectional semiaxes being 0.08 $(\frac{1}{2}b_0^*)\times0.33$ $(\frac{1}{2}d_0^*)$ or 0.07×0.12 Å^{-1}. The volume of this ellipsoid amounts to 2.5% of the Brillouin zone.

The $2a_0, 2c_0$ periodic lattice distortion which develops in $TiSe_2$ comes as a result of electron-hole coupling between carrier pockets at L and Γ on a particularly simply Fermi surface. The absence of any such distortion in $TaSe_3$ might be ascribed to the clearly greater complexity of its Fermi surface. When we come below to examine the form expected for the band structure of $TaSe_3$ it will be seen that both p- and d-band carriers are indeed anticipated. We do not believe either that the $2b_0$ repeat found in NbS_3 could be due to ΓZ electron-hole interaction, because that distortion amounts not to anion-cation sublattice coupling, but rather to cation-cation, and the latter is of more general nature as was emphasized earlier.

We have already noted in the beginning of Sec. II the manner in which $TaSe_3$ is nearly rendered semiconducting. The anion sublattice of the orange column takes four electrons per Ta(Se_2)Se unit, the red column six electrons per $TaSe_3$ unit, so that, with 10 electrons given over per pair of Ta, the joint tantalum-based d band is drained of electrons. That this process is not in practice quite carried to completion is due to slight overlap between the top of the p band and the bottom of the d band. Such overlap indeed exists in 2H-$TaSe_2$ (as detected by photoelectron spectroscopy), but

is not for that d^1 compound able to affect (directly) the Fermi surface. Because in $TaSe_3$ the tantalum valence is larger than in $TaSe_2$, the d band will actually be withdrawn $\sim\frac{1}{2}$ eV to higher energies. However, this tendency for the p-d band overlap to be lost is amply countered by the destabilization of the top of the p band in $TaSe_3$ relative to $TaSe_2$, for weakly antibonding p states now are present in the red column (and possibly between red and orange columns; Se-Se 2.65 Å). (The antibonding p states from the orange column are unoccupied and probably lie 2–3 eV above the Fermi level.)

Above we have seen that both types of Ta are rendered d^0, i.e., 5+ in ionic terms. However, since the balancing coordination charge in the orange prisms is "4–" and in the red prisms "6–", the d-band state associated with the latter will lie to higher energy. It would seem then, that the observed electron content carried by the lowest d band is to be associated in the main with the orange columns. It should be remembered, however, that the anion sublattices of the two columns are not independent, and that p-d hybridization is substantial. The holes, though to a still lesser degree, one might associated with the red columns. Hole anisotropy in the slabs should be appreciably less than electron anisotropy.

The rather large number of orbits detected in the SdH work follows from there being two atoms of each of the eight kinds per unit cell. This secures a dual presence at a great many points in the zone for the bands that are based on any given atomic function, say, orange tantalum d_{z^2}. The Fermi surface probably incorporates bits from the latter two bands and from at least two sets of p bands, so with neck and belly orbits possible we soon reach a large number.

There is no evidence from its various properties of any transition occurring in $TaSe_3$ between 4 and 700 °K.[1(b),5(a)] The situation with regard to superconductivity is not clear.[9,12,16]

(ii) $NbSe_3$. In the SdH work it was found that $NbSe_3$, contrary to $TaSe_3$, showed only one primary (i.e., nonharmonic) orbit, and that very small.[11,16,23] The orbit also takes an unusual rotated angular aspect relative to those for $TaSe_3$. The size is only about $\frac{1}{10}$ of the size of orbit 4 in $TaSe_3$. The occupied volume of k space is thus going to be down by a factor $\sim\frac{1}{30}$. This amounts to a 0.1% filling of the $NbSe_3$ zone, or close to the same number of carriers as was suggested by the Hall constant, namely $4\times10^{18}/cm^3$. These are the carriers left following the periodic-structural-distortion (PSD) interactions that set in at 144 and 59 °K, from which ~75% of the original carrier content is lost.

The electronic condition actually prevailing in $NbSe_3$ at 300 °K is also necessarily significantly different from that in $TaSe_3$. The added presence in the structure of the yellow columns means there is now a smaller percentage demand upon the d levels for electrons to complete the p band of the depaired, red-column anion sublattice. The reckoning goes as follows: The six cations per cell introduce 30 outer electrons. Of these 4×4 electrons are required by the two pairs of orange and yellow Se_2^{2-} containing units. The pair of red $NbSe_3$ units then require a further 2×6 electrons. This leaves over for the d band two electrons. The lowest reaching d band will be one of the two d_{z^2}-based bands associated with the yellow columns. The observed noninsulating character of $NbSe_3$ can readily be accepted on the following counts: First, the two yellow bands are going to be tied together by symmetry at certain points in the zone. Second, the lowermost d_{z^2} band associated with the orange column is likely also to pass below the Fermi level. Third, the top of the p band may continue to overlap E_F, despite the latter now being raised significantly into the d band (unlike in $TaSe_3$). This is because the general d-p separation in the $4d$ material will be reduced by $\sim\frac{1}{3}$ eV relative to the $5d$ (see Ref. 47 for the case of $NbSe_2$ vs $TaSe_2$, etc.).

It should be noted that in the absence of d-d and p-d overlap, an electron content of exactly 1 electron per yellow cation could possibly have brought *full* cation-cation pairing to the yellow columns, as in NbS_3. Loss of the integral electron number per yellow cation counters this, as also must the crystal strain energy since only two of the six columns would show pairing. The distortions actually found in $NbSe_3$ seem in fact, as we shall see below, to be seated both in the yellow and the orange columns.

It is possible that the greater dispersion of the yellow-based d band (from the continuous yellow connectivity in the a_0 direction) allows the orange band to become significantly filled too, despite its lowermost point being higher in energy. One may in fact infer from the diffraction results that the extents of k space over which the two bands lie below the Fermi level are rather similar. In those circumstances both types of chain will contain only about $\frac{1}{2}$ electron per niobium.

What the diffraction experiments[14,21,22] reveal is that the 144-°K transition leads to a distortion with wave vector (0, 0.243, 0) while the second transition at 59 °K leads to an independent distortion with wave vector (0.5, 0.263, 0.5). The former PSD one may associate with the yellow columns. Those columns define near-neighbor sheets parallel to the a axis. The second PSD can be associated with the orange columns, which define much more

loosely related sheets having the 101 orientation (see Fig. 5). The phasing between neighboring centers of inversion within the a-c plane for the yellow column wave is uniformly 0°, but for the orange-column wave in the 101 direction (i.e., across the yellow sheets) it is π. (Remember within a duo of columns the two are staggered by one-half a prism height about the intervening center of inversion.)

Along the columns both waves are seen to be incommensurate. The wavelengths invert out as 4.115 and 3.802 b_0, respectively. The closeness of these periodicities to each other and to $4b_0$ offers suggestion for the driving mechanism behind these distortions.

The sort of band-structure situation that we have envisaged above is portrayed in Fig. 8. A hybridization gap, following band crossing of the lowermost yellow and orange bands near $\frac{1}{2}\,\overrightarrow{\Gamma Z}$ is shown leading to the appearance of holes in that region. Compensating electron pockets are introduced at Γ and Z. From such a semimetallic situation 75% of the carriers are subsequently eliminated under the distortions. Since the distortions each grow from zero in a BCS-like fashion,[22] it has been presumed that the loss of carriers arises from Fermi-surface nesting and gapping through development of two independent charge-density waves

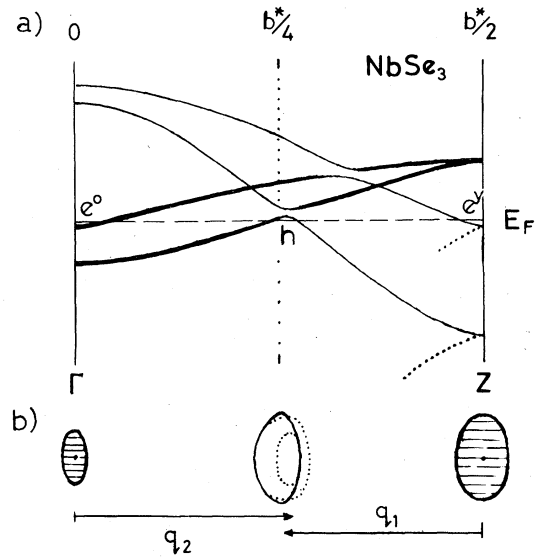

FIG. 8. Type of band structure envisaged for $NbSe_3$, light bands being associated with d_{z^2} of the yellow columns, heavy bands with d_{z^2} of the orange columns, and dotted bands with occupied slightly antibonding p states. In the lower part of the figure is indicated how the majority of electrons and holes may be eliminated from this semimetallic situation under nesting in the yellow column by $\vec{q}_1$ and in the orange column by $\vec{q}_2$. The size of the pockets is magnified for clarity.

with wave vectors q_1 and q_2. Figure 8 indicates how the gapping can first set in with the yellow-column carriers, and then extend to the orange.

We have much reservation, though, about using an excitonic insulator description of this type for the present case. It is unfortunate that substitutional doping in an isostructural, rigid-band framework is not an available probe here (unlike 1T-$TaSe_2$). The fact, however, that a $4t_0$ periodicity occurs again in TaS_3 (Refs. 13, 15, 21, and 25) where the structure is different, and that one sees the endemic $2t_0$ periodicity from cation pairing in the columns of NbS_3, opens an alternative avenue to investigation—metal-metal bonding.

Under nesting and gapping only band states fairly close to the Fermi level are stabilized. By contrast, the cation pairing process leads to stabilization of states throughout the bonding band. Normally this stabilization in a linear-chain compound like $V(S_2)_2$, NbI_4, or $RuBr_3$ is so great that the pairing cannot be removed thermally. This likewise is true for NbS_3. In some cases like VO_2 and NbO_2, which are not crystallographically one dimensional, the pairing may be removed thermally, normally involving a first-order transition. The cation displacement associated with pairing in $V(S_2)_2$ is 0.20 Å[41] and in NbS_3 0.16 Å,[20] but for VO_2 it is only 0.12 Å.[45]

In $NbSe_3$ the number of d-electrons in the yellow and orange columns is sufficient there only to pair up every second couple of cations. This, plus the fact that the electron count per (orange and yellow) cation is not quite $\frac{1}{2}$, and that the red columns are not participating, would explain why for such behavior in $NbSe_3$ the distortions grow in second-order fashion. One can also accommodate the fact that the incommensurate distortions which arise here, although only marginally removed from $q_b = \frac{1}{4}$, do not lock-in during cooling. Indeed, unlike closely commensurate 2H-$TaSe_2$ or 1T-TaS_2,[53] the wave vectors in $NbSe_3$ are found to be invariant with temperature.[22] One may suspect that the observed wave vectors are simply approximations to the vulgar fractions $\frac{9}{37}$ (i.e., 0.2432, with $\lambda_1 = 4\frac{1}{9}b_0$) and $\frac{5}{19}$ (i.e., 0.2632, with $\lambda_2 = 3\frac{4}{5}b_0$), implying that in $NbSe_3$ we are dealing with a "discommensurate" situation[54] which is strongly imposed. The implied situation in the yellow chains ($e \lesssim \frac{1}{2}$) is that pairing between every second couple of niobium atoms proceeds undisturbed for nine periods before an extra unpaired atom or discommensuration appears, as in Fig. 9. In the orange columns the electron count ($e \gtrsim \frac{1}{2}$) is conversely such that only one unpaired niobium is present at the end of five undisturbed periods. With these defects repeating regularly every 37 and 19 atoms the diffraction is as from the recorded incommen-

surate waves. However, in nonsinusoidal situations like this, higher harmonics must show up (see Ref. 53 for the case of $2H$-$TaSe_2$). In $NbSe_3$ a second harmonic is in fact reported[22] with $I_2 = 0.01\ I_1$.

The red columns should, through the above processes, show no cation pairing. The only measurements so far indicate that the lateral dimensions in a red column increase[21] (though it must be remembered that the low-temperature crystallographic refinement is of an averaged structure).

(iii) TaS_3. TaS_3 has long been known to undergo a semimetal to semiconductor transition around 200 °K.[1] Until the structure of TaS_3 is resolved, it is not possible to interpret in detail what is happening electronically. The here commensurate $4c_0$ period along the chains could even be due to a complex packing of fully paired chains. (N.B. $a' = 2a_0$; $b' = 8b_0$: Ref. 25.) The distortion develops through a long precursor range down from room temperature, before long-range order appears around 220 °K.[13,21,25] In $TiSe_2$ (Ref. 52) similarly strong scattering preceeds the adoption of a commensurate distortion. In neither case is the diffuse scattering entirely lost at the transition. The transition in TaS_3 appears to wipe out the entire Fermi surface, producing an electrical activation energy of 0.15 eV.[13] The residual conductivity ~3 $(\Omega - \text{cm})^{-1}$ probably comes from poor stoichiometry.

IV. SLIDING WAVES IN $NbSe_3$: A UNIQUE SITUATION

What has proved so far unique about $NbSe_3$ among CDW-bearing materials is that its CDW-PSD's can be induced to slide and thereby carry current under a very small applied electric field.[8,10] Ease of sliding of course requires that the CDW be incommensurate (i.e., not locked-in to the parent lattice), and also that its pinning by impurities and defects be low. It is in this later area that $NbSe_3$ is exceptional.

The trichalcogenides appear to have a very narrow homogeneity range, quite unlike the dichalcogenides. This is probably because the crystal structures are so complex and are "molecularized" in a fashion specifically determined by the atoms and stoichiometry of the compound. It is likely that substitutional defects are thereby held to a minimum [compare "VS_2" with $V(S_2)_2$]. Beyond this in $NbSe_3$ we have an internal sink for impurities, namely, the red column. By far the most common impurity cation likely to be incorporated is Ta, and this would certainly prefer the latter's higher valency situation. Anion impurities would also favor the red columns, not being readily able to participate in the anion pair bonding of the other columns. By residing on the red columns, an anion impurity can also avoid having to participate in the intercolumn pathways of the eightfold Nb coordination. The drive to establish that coordination also probably restricts the inclusion of cation vacancies on the yellow and orange columns. Indeed the anion array of $NbSe_3$ is not at all based on close packing. Cation vacancies *are* found in the hcp anion-arrayed chain structure of HfI_3,[55] and help to inhibit the expected metallic conductivity ("broken strands"). It should be remembered, too, that the (O and Y) chains in $NbSe_3$ occur in interconnected "duos," so that any cation vacancy which is incorporated into one of these chains may be more readily by-

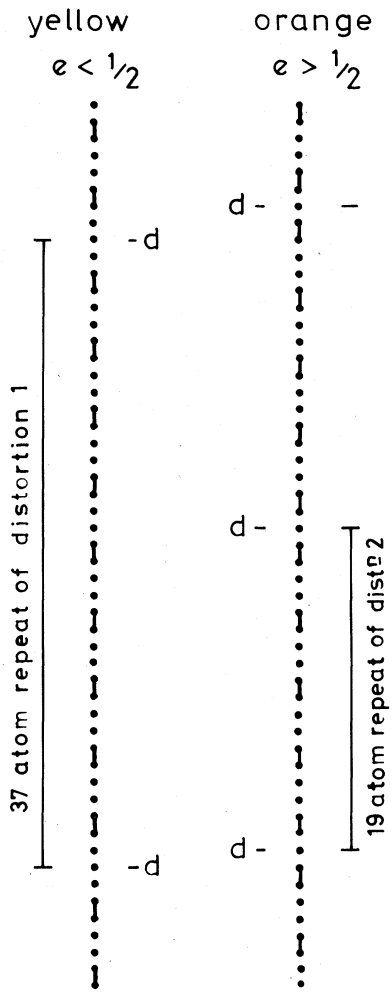

FIG. 9. Model of alternate pairing of Nb atoms in yellow and orange columns of $NbSe_3$. Deviation of the average electron content per cation there from $\frac{1}{2}$ is taken up in the discommensurations (d). The latter will slide through the columns by bond flipping. The crystallographic distortions grow in second-order fashion. In this model the details of the Fermi-surface geometry are not important, electronic counting being sufficient.

passed.

As a result of all these factors, $NbSe_3$ ends up by presenting very high single carrier mobilities[30] for a semimetallic transition metal compound. This mirrors the ease with which the collective mode is depinned. What is envisaged as happening in the motion of the latter is that the discommensurations propagate as solitons through a flipping over of each successive electron-pair bond along the column (see Fig. 9). The "sliding" is found to leave the amplitude and wave vector of the PSD unchanged[22] (in addition to the onset temperature), implying that the process is cooperative between chains, probably being strain coupled across the many centers of inversion of the parent structure. The fact that the discommensurations in the orange and yellow chains have to appear at different intervals restrains the structure from excessive distortion, as must the presence of the inactive red columns.

It is this general conglomeration of unusual features in the structure and chemistry of $NbSe_3$ which make it difficult to envisage another material more suited to the appearance of sliding "charge-density waves." One certainly would not expect it in Zr-substituted NbS_3, where the nonintegral electron count is produced only at the expense of introducing a strong pinning center if the column. One possibility may be to boost the d-band electron content in $TaSe_3$ by pressure.

Under pressure $NbSe_3$ rapidly loses its PSD's; the amplitudes falling in addition to there being a depression of both onset temperatures at the rate of 4 K/kB.[6] This is not surprising since pressure in these compounds more than most will modify the band structure. Actually $NbSe_3$ rather quickly becomes superconducting.[9] The greatest sensitivity is seen as coming from the top of the p band. A couple of the nonbonding intercolumn Se-Se distances are particularly short (2.73 and 2.9 Å), and these, together with the states from the red-column Se-Se pair that we have regarding as weakly bonded, should develop stronger bonding-antibonding characteristics. Little change is needed to carry the latter occupied states above the Fermi level. So there should arise a rather rapid transfer of electrons from the anion to the cation sublattice, destroying the electron count and/or geometry of the Fermi surface which originally drove the distortions (see Fig. 8). It would, during this process, be of great interest to know what happens to the distortion wave vectors. Does the yellow column wave ever lock-in to $4b_0$? It has been observed that the upper transition, which we have associated with the yellow column, initially has its amplitude reduced more slowly than does the lower.[6] If there are indeed discommensurations of the type suggested by the pair-bonding picture then the wave vectors should change by small but finite jumps, going from $\frac{1}{4}\times\frac{36}{37}$ (or 0.2432) to $\frac{1}{4}\times\frac{40}{41}$ (or 0.2439), etc., and from $\frac{1}{4}\times\frac{20}{19}$ (or 0.2632) to $\frac{1}{4}\times\frac{16}{15}$ (or 0.2666), etc. as electrons pass from the p into the d band.

V. SUMMARY

By examining the structure and bonding of the transition-metal trichalcogenides in more detail than previously, it has proved possible to obtain a better understanding of the electronic properties of these materials. It is seen how those properties come to be significantly different from material to material. $TaSe_3$ is a semimetal by p-d overlap, $NbSe_3$ by d-d overlap. The number of free carriers is significantly greater in $TaSe_3$, but the number of electrons actually in the d band is greater in $NbSe_3$. The latter number amounts to very close to $\frac{1}{2}$ an electron per cation in the columns showing Se-Se pairs. These electrons are responsible for the two periodic structural distortions which develop in $NbSe_3$. The upper transition we associate with the columns having the tightest Se-Se pairing that form sheets parallel to a_0, and have a broader, lower-reaching d band. It is concluded that these distortions are better described by a discommensurate array of cation pair bonds than by a traditional CDW, its geometry strictly determined by that of the Fermi-surface Kohn anomalies. While the Fermi surface of these materials is not fully determined, it is clear that these materials should not be regarded as linear-chain metals after the fashion of KCP and TTF-TCNQ. The trichalcogenides clearly provide a challenge to band theorists using new methods which may be able to yield meaningful results for unit cells of this size and complexity. The effect of the several variable anion-anion pair interactions should be interesting to follow. It is not going to be possible to neglect many of the intercolumn Se-Se interactions, in addition to the M-X coupling of the eightfold cation coordination.

With this background we are finally able to see why the distortions in $NbSe_3$ are so weakly pinned to the lattice by impurities or defects. The sliding of these distortions we model in terms of bond flipping into the discommensurations.

What the bond model does, of course, is to select for the periodic structural distortion a specific phasing relative to the crystal lattice within the commensurate segments between discommensurations. Figure 10(a) identifies that phasing as $-\frac{1}{4}\pi$. Figure 10(b) shows the situation for $\phi = 0$, appropriate to a discommensurate charge-density wave with charge maxima and minima centered about cation sites rather than between them.

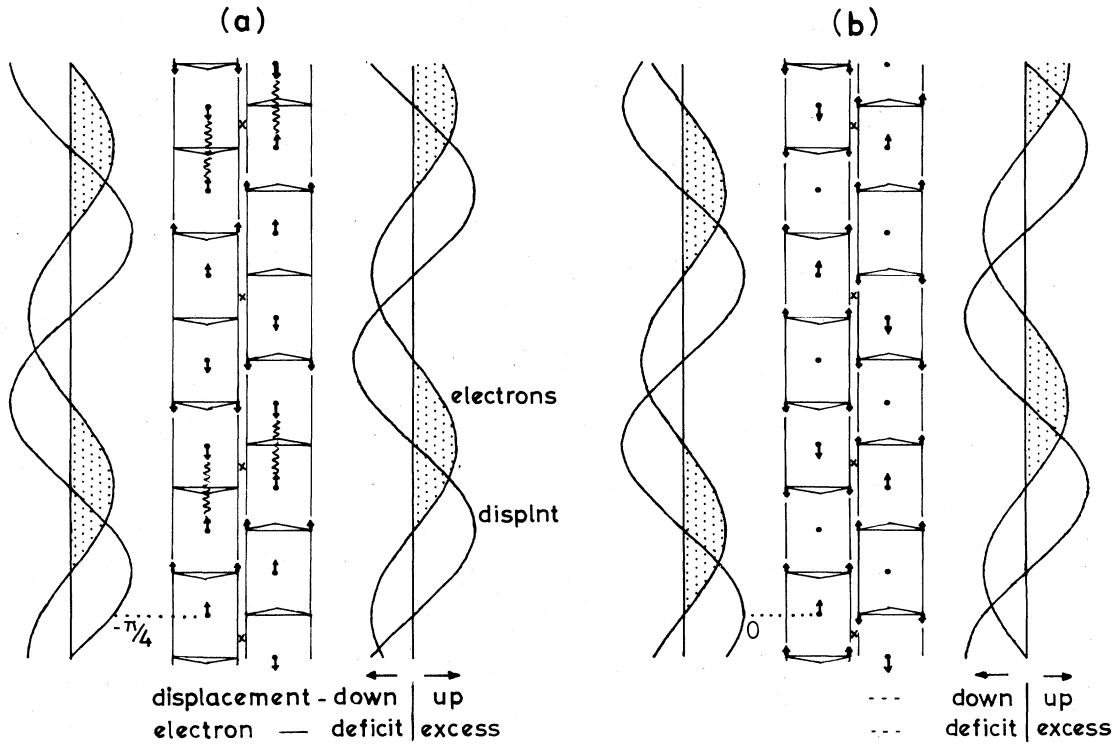

FIG. 10. (a) Phasing of a cosine wave (for the origin chosen) that is appropriate to the bonding model is $-\frac{1}{4}\pi$. Alternate pairs of atoms approach and separate. The corresponding charge wave brings electrons into the bond region. In practice the waves will deviate progressively from sinusoidal form as the amplitude of the distortion increases; (b) This shows the phasing $\phi = 0$, which produces electron excess on every fourth cation. Here the two chains of the duo are given a relative phasing most suited to the dominance of electrostatic stacking. In Fig. 10(a) the duo were shown with the relative phasing more suited to the dominance of strain coupling.

It must finally be recalled that the active yellow and orange columns occur in duos, these being separated by the red columns. The two columns in each duo are staggered relative to each other by half the height of a prismatic unit. Figure 10 portrays our suspicion that the wave phasing within a duo will, because of the approach to eightfold coordination, be determined more by lattice strain than by electrostatic considerations. As within a single column, the strong cation motions bring in train anion motions that are principally determined by the need to maintain the M-X bond lengths and the p-band energetics. The working out of this principle was very evident in the relative anion-cation sublattice phasing and distortion pattern for the crystallographically much simpler case of $2H$-$TaSe_2$.[48] In the present case the complex parent crystallography denies effective modeling and analysis of the available diffraction data for the low-temperature state.

[1](a) S. Furuseth, L. Brattas, and A. Kjekshus, Acta Chem. Scand. A 29, 623 (1975); (b) L. Brattås and A. Kjekshus, *ibid.* 26, 3441 (1975).
[2]W. Schairer and M. W. Shafer, Phys. Status Solidi A 17, 181 (1973).
[3]F. Jellinek, R. A. Pollack, and M. W. Shafer, Mater. Res. Bull. 9, 845 (1974).
[4]A. Meerschaut and J. Rouxel, J. Less Common Met. 39, 197 (1975).
[5](a) P. Haen, P. Monceau, B. Tissier, G. Waysand, A. Meerschaut, P. Molinie, and J. Rouxel, Proc. Low Temp. 14 5, 445 (1975); (b) Ferroelectrics 17, 447 (1977).
[6]J. Chaussy, P. Haen, J. C. Lasjaunias, P. Monceau, G. Waysand, A. Waintal, A. Meerschaut, P. Molinie, and J. Rouxel, Solid State Commun. 20, 759 (1976).
[7]P. Haen, G. Waysand, G. Boch, A. Waintal, P. Monceau, N. P. Ong, and A. M. Portis, J. Phys. (Paris) Colloq. 37, C4-179 (1976).
[8]P. Monceau, N. P. Ong, A. M. Portis, A. Meerschaut, and J. Rouxel, Phys. Rev. Lett. 37, 602 (1976).
[9]P. Monceau, J. Peyrard, J. Richard, P. Molinie, Phys. Rev. Lett. 39, 161 (1976).
[10]N. P. Ong and P. Monceau, Phys. Rev. B 16, 3443

(1977).
[11]P. Monceau, Solid State Commun. 24, 331 (1977).
[12]T. Sambongi, M. Yamamoto, K. Tsutsumi, K. Shiozaki, K. Yamaya, and Y. Abe, J. Phys. Soc. Jpn. 42, 1421 (1977).
[13]T. Sambongi, K. Tsutsumi, K. Shiozaki, M. Yamamoto, K. Yamaya, and Y. Abe, Solid State Commun. 22, 729 (1977).
[14]K. Tsutsumi, T. Takagaki, M. Yamamoto, Y. Shiozaki, M. Ido, T. Sambongi, K. Yamaya, and Y. Abe, Phys. Rev. Lett. 39, 1675 (1977).
[15]G. van Tendeloo, J. van Landuyt, and S. Amelinckx, Phys. Status Solidi A 43, K137 (1977).
[16]R. M. Fleming, J. A. Polo, Jr., and R. V. Coleman, Phys. Rev. B 17, 1634 (1978).
[17]N. P. Ong, Phys. Rev. B 17, 3243 (1978).
[18]J. W. Brill and N. P. Ong, Solid State Commun. 25, 1075 (1978).
[19]N. P. Ong and P. Monceau, Solid State Commun. 26, 487 (1978).
[20]J. Rijnsdorp and F. Jellinek, J. Solid State Chem. 25, 325 (1978).
[21]J. L. Hodeau, M. Marezio, C. Roncan, R. Ayroles, A. Meerschaut, J. Rouxel, and P. Monceau, J. Phys. C 11, 4117 (1978).
[22]R. M. Fleming, D. E. Moncton, and D. B. McWhan, Phys. Rev. B 19, 5560 (1978).
[23]P. Monceau and A. Briggs, J. Phys. C 11, L465 (1978).
[24]J. C. Tsang, C. Hermann, and M. W. Shafer, Phys. Rev. Lett. 40, 1528 (1978).
[25]K. Tsutsumi, T. Sambongi, S. Kagoshima, and, T. Ishiguro, J. Phys. Soc. Jpn. 44, 1735 (1978).
[26]S. Nakamura and R. Aoki, Solid State Commun. 27, 151 (1978).
[27]F. J. DiSalvo (unpublished).
[28]N. P. Ong and J. W. Brill, Phys. Rev. B 18, 5265 (1978).
[29]N. P. Ong, Phys. Rev. B 18, 5272 (1978).
[30]P. A. Lee (unpublished).
[31]T.R. Koehler and P. A. Lee, Phys. Rev. B 16, 5263 (1977).
[32]M. L. Boriack and A. W. Overhauser, Phys. Rev. B 16, 5206 (1977).
[33]J. B. Sokoloff, Phys. Rev. B 16, 3367 (1977).
[34]P. A. Lee, T. M. Rice, and P. W. Anderson, Solid State Commun., 14, 703 (1974).
[35]J. A. Wilson, F. J. DiSalvo, and S. Mahajan, Adv. Phys. 24, 117 (1975).
[36]F. Hulliger, *Structural Chemistry of Layer Type Phases*, Vol. 5 of *Physics and Chemistry of Materials with Layered Structures*, edited by F. Lévy (Reidel, Dordrecht-Holland, 1976).
[37](a) E. Bjerkelund and A. Kjekshus, Z. Anorg. Allg. Chem. 328, 235 (1964); (b) E. Bjerkelund, J. H. Fermor, and A. Kjekshus, Acta Chem. Scand. 20, 1836 (1966).
[38]F. Kadijk and F. Jellinek, J. Less Common Met. 19, 421 (1969).
[39]P. Brüesch, S. Strässler, and H. R. Zeller, Phys. Rev. B 12, 219 (1975), and references therein.
[40]H. Kawamura, I. Shiorotani, T. Tachikawa, Phys. Lett. A 65, 335 (1978).
[41](a) R. Allmann, I. Baumann, A. Kutoglu, H. Rösch, and E. Hellner, Naturwissenschaften 51, 263 (1964); (b) W. Klemm and H. G. Schnering, *ibid.* 52, 12 (1965).
[42]R. Pynn, J. D. Axe, and P. M. Raccah, Phys. Rev. B 17, 2196 (1976), and references therein.
[43]R. N. Bhatt, Phys. Rev. B 17, 2947 (1978), and references therein.
[44]H. G. Schnering and W. Beckmann, Z. Anorg. Allg. Chem., 347, 231 (1966).
[45]E. Caruthers and L. Kleinman, Phys. Rev. B 7, 3760 (3753) (1973) and references therein.
[46](a) J. A. Wilson, *Proceedings of the Conference on Phase Transitions*, edited by L. E. Cross (Pergamon, New York, 1973), pp. 101–116; (b) J. A. Wilson, Adv. Phys. 21, 143 (1972).
[47]J. A. Wilson and A. D. Yoffe, Adv. Phys. 18, 193 (1969).
[48]J. A. Wilson, Phys. Rev. 17, 3880 (1978).
[49]A. Kjekshus, T. Rakke, and A. F. Andresen, Acta Chem. Scand. A 28, 996 (1974), and references therein.
[50]K. Tsutsumi (private communication).
[51]L. F. Mattheiss, Phys. Rev. B 8, 3719 (1973). This examines case of $TaSe_2$, etc. in some detail.
[52]J. A. Wilson, A. S. Barker, F. J. DiSalvo, and J. A. Ditzenberger, Phys. Rev. B 18, 2866 (1978), and references therein.
[53]K. Nakanishi and H. Shiba, J. Phys. Soc. Jpn., 44, 1465 (1978).
[54]W. L. McMillan, Phys. Rev. B 14, 1496 (1976).
[55]A. W. Struss and J. D. Corbett, Inorg. Chem. 8, 227 (1969).
[56]J. A. Wilson, Phys. Rev. B 15, 5748 (1977).